# Melting Process and Mechanism for Vibration Induced Single-Screw Extruder

**Guang-Sheng Zeng, Jin-Ping Qu, Yan-Hong Feng**

*National Engineering Research Center of Novel Equipment for Polymer Processing, The Key Laboratory of Polymer Processing Engineering, Ministry of Education, South China University of Technology, Guangzhou 510641, China*

Received 20 June 2006; accepted 14 October 2006
DOI 10.1002/app.25721
Published online in Wiley InterScience (www.interscience.wiley.com).

**ABSTRACT:** The effect of a vibration force field on the melting process of an extruder is studied. It is shown that the mechanism for melting differs from conventional theory. Experimental studies of melting of low-density polyethylene (LDPE) pellets in a vibration-induced single-screw (VISS) extruder show that melting is initiated on the inside of the barrel and the surface of screw. Models were developed that explain the melting mechanism in those regions. The melting at the surface of the screw is mainly initiated by frictional work on the pellets by the vibration and rotation of the screw. The melting action at the barrel is induced by a barrel temperature higher than the melting point and propagated by viscous dissipation heating of the melt film produced. The theory is supplemented by a calculation sample, which shows good agreement with experimental data obtained on a transparent barrel VISS (T-VISS) extruder and a half-open barrel VISS (H-VISS) extruder with LDPE. The results of the experiment and calculation sample indicate that the introduction of vibration-induced field can improve the melting capacity of extruder to a great extent. The present model enables the prediction of processing parameters for VISS extruders, from which the optimum operating conditions can be obtained.  J Appl Polym Sci 104: 2504–2514, 2007

**Key words:** melting model; extruder; LDPE; screw vibration

## INTRODUCTION

One of the major tasks for most extruders is the melting of a solid feed whether it is in the form of pellets or powder. This is true for both VISS extruders and conventional extruders. Although melting in conventional extruders has been extensively studied and modeled, very little information has been presented on the mechanism of melting that occurs in VISS extruders.

The foremost theoretical framework for analyzing the melting process in single-screw extruders was established by Tadmor and coworkers in the late 1960s.[1,2] Their model developments were based on experimental observations first reported by Maddock,[3] and later confirmed by other researchers.[4–8] In brief, these experiments indicated that during the course of melting the solid bed is located against the trailing flight, the melt pool accumulates along the pushing flight, and a thin melt film separates the barrel and the solid bed. As melting proceeds, the melt pool gradually grows at the expense of the solid bed until eventually the melted material fills the entire cross section of the screw channel.

Although Tadmor's melting mechanism appears to be quite general for most extruders, some significant exceptions have been reported. Menges and Klenk[9] observed a situation related to PVC extrusion in which the melt pool formed at the trailing side instead of the pushing side of the screw flight. Dekker,[10] on the other hand, did not detect a distinct melt pool at all; rather, the solid bed was surrounded by melt on all sides. This phenomenon was explained clearly and modeled by Lindt.[11,12]

In the Lindt's model, the melt is considered to accumulate chiefly in the film surrounding the solid bed rather than forming a significant pool at the flight wall. The temperature of both the barrel and the screw surfaces exceed the melting point of the polymer i.e., the pressure drop and speed in cross-channel are neglected, and the leakage flow across flights is taken into consideration.[11,12]

Lee and Han[13] summarized several models provided by Tadmor (and his coworkers) and Lindt's group to describe the melting process occurring in single-screw extruders, and they developed a new model to predict the deformation and movement of the solid bed surrounded by its melt in single-screw extruders. In their model, they considered the breakup of the polymer solid bed, and advanced the

*Correspondence to:* J.-P. Qu (jpqu@scut.edu.cn).
Contract grant sponsor: National Natural Science Foundation of China; contract grant numbers: 20074010, 10472034, 10590351, 20027002.
Contract grant sponsor: National Natural Science Equipment Foundation of China; contract grant number: 20027002.
Contract grant sponsor: Doctorate Foundation of South China University of Technology.

theory of breakup of a solid bed. Additionally, experimental and theoretical studies on the melting of twin-screw extruder have appeared and achieved significant progress.[14,15]

Contrary to the melting theory of conventional extruders, few publications about the melting theory of VISS extruders can be found. The objective of this work is ultimately to determine the effect of a vibration force field on the melting process of VISS extruder. To achieve this goal, both experimental and modeling studies is performed.

## MELTING MODEL

### Physical model

The VISS extruder has been widely used for thermoplastics processing since the 1990s,[16–20] and has since provided a significant benefit to society while reducing costs. The VISS extruder screw can vibrate along the axial direction as it is rotating. This generates a vibration force field that propagates throughout the whole polymer extrusion. As a result of the impact from the vibration force, the melting process becomes dynamic and time-dependent.

The present model is based on previous experimental observations,[21] which is depicted schematically in Figure 1 together with the coordinate system used. The geometrical size of the screw is shown in Figure 1(a), in which $N$ is the rotation speed of screw, and $\xi = A \sin(\omega t)$ is the screw vibration along the axial direction. Figure 1(b) is the melting mechanism used in this work. As shown in Figure 1(b), in the cross section of screw channel, the polymer solid bed is surrounded by melted polymer, similar to the Lindt model, and the melt is flowing along outside of the solid bed. The heat necessary for the phase conversion is supplied by two sources, from the hot barrel and from viscous dissipation or internal friction. Because of the effect of vibration force field, the heat generated by viscous dissipation may be significant enough to even out the temperature distribution in polymer melt and avoid localized superheating. As melting proceeds, the thickness of melt gradually grows at the expense of the solid bed until eventually the melted material fills the entire cross section of the screw channel. When the extruder is running under stable conditions (rotation speed and vibration parameters are constant), the length of melting section and the distribution of solid-bed will be unvaried, therefore, the speed of the polymer pellets entering the barrel is equal to the melting rate, as well as the output rate of the extrusion. Hence, melting capacity of the extruder can be improved by an increase in the growth rate of the melt or a decrease in the length of the melting section.

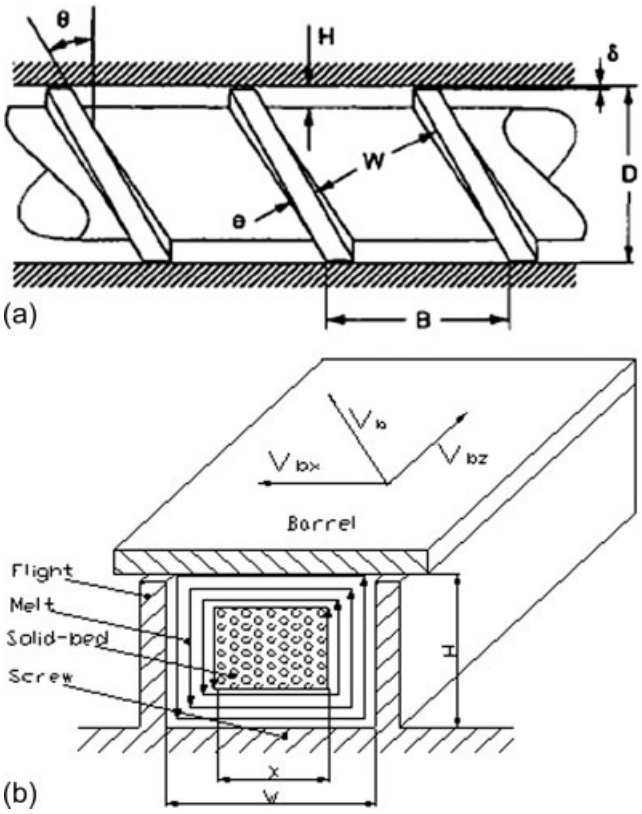


**Figure 1** Melting model in vibration extruder: (a) Illustration of the geometrical size of screw; (b) Melting mechanism and coordinate system used in this work.

### Mathematical analytical model

The theoretical analysis presented here deals with the major part of the melting section where the temperature of both the barrel and screw (include the flight) surfaces exceed the melting point of the polymer, and the solid bed becomes entirely surrounded by melt. At the start point of the melting section, we let $z = 0$, where $z$ is the down screw channel direction [Fig. 1(b)].

The analytical model has been obtained, using the following general assumptions:

1. The melting mechanism of Figure 1 applies;
2. The interfaces involved are smooth and at determinate physical conditions;
3. The screw channel can conceptually be unrolled and described by a local Cartesian system (Fig. 1);
4. The velocity along the depth of polymer melt is negligible;
5. The polymer melt is incompressible;
6. Barrel is mobile, and screw is fixed relatively;
7. Leakage flow from the flights is negligible.

From the assumptions above, we find that the rotation and vibration velocity of screw changes

with the relative speed of the inside surface of barrel. The following equations are then obtained:

$$V_b = \pi DN \tag{1}$$

$$V_{bz} = V_b \cos\theta \tag{2}$$

$$V_{bx} = V_b \sin\theta \tag{3}$$

$$\xi = A \ \sin(\omega t) \tag{4}$$

$$V_d = \frac{d\xi}{dt} = A\omega \ \cos(\omega t) \tag{5}$$

$$V_{dx} = V_d \ \cos\theta \tag{6}$$

$$V_{dz} = V_d \ \sin\theta \tag{7}$$

where $D$ is the outer diameter of screw, $N$ is the rotation speed of screw, $V_b$ is the relative speed of the inside of the barrel, $V_{bz}$ and $V_{bx}$ are the branch speed of $V_b$ along $z$ and $x$ direction, respectively, $\theta$ is the screw flight angle, $V_d$ is the speed generated by the axial vibration of screw, which can be split into branch speeds $V_{dx}$ and $V_{dz}$ along the $x$ direction and $z$ direction, respectively, $A$ is the vibration amplitude, $\omega = 2\pi f$ is the angular frequency and $f$ is the frequency.

Moreover, since the thermal conductivity of polymer material is generally low (about 0.29 W/mK), the melt is flowing along the solid bed, with convection heat prevailing. Therefore, we can assume that at the melting section of screw, the inside of barrel and the screw surface are at the same temperature. Hence, we can approximately unwrap the polymer solid-bed from its centerline. This allows us to simplify the melt flowing model as shown in Figure 2. The upper plate is a hot wall (it denotes the inside of barrel or the screw surface), and is moving at the speed of $V_x$ and $V_z$, the other plate denotes the solid bed, which is fixed. $v_x$ and $v_z$ are the velocity distributions in the thickness of melt film along the $x$- and $z$-direction, respectively, $y$ is the direction along the thickness of melt film. $V_x$ and $V_z$ are given below:

$$V_x = V_b \ \sin\theta + V_d \ \cos\theta \tag{8}$$

$$V_z = V_b \ \cos\theta + V_d \ \sin\theta - V_{sz} \tag{9}$$

where $V_{SZ}$ is the velocity of solid-bed along screw channel direction, and then the momentum equation is obtained:

$$\rho_m \frac{dv_z}{dt} = \frac{\partial \tau_{zy}}{\partial_y} - \frac{\partial P}{\partial z} \tag{10}$$

$$\rho_m \frac{dv_x}{dt} = \frac{\partial \tau_{xy}}{\partial_y} - \frac{\partial P}{\partial x} \tag{11}$$

where $\tau_{zy}$ and $\tau_{xy}$ are the shear stress generated by the screw's rotation and vibration, $\rho_m$ is the density of polymer melt, $t$ is the time, $P$ is the pressure.

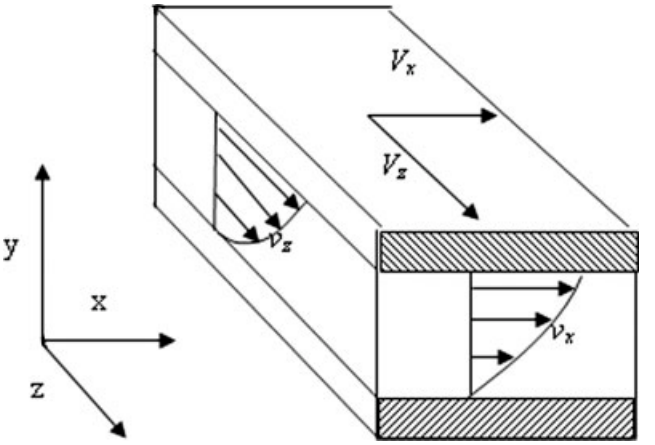


**Figure 2** Model of polymer melt flow.

The power-law constitutive equation:

$$\tau_{yz} = m_0 \ \exp[a(T - T_m)]\mathrm{I}_2^{(n-1)/2} \frac{dv_z}{dy} \tag{12}$$

$$\tau_{xy} = m_0 \ \exp[a(T - T_m)]\mathrm{I}_2^{(n-1)/2} \frac{dv_x}{dy} \tag{13}$$

$$\mathrm{I}_2 = \left(\frac{dv_x}{dy}\right)^2 + \left(\frac{dv_z}{dy}\right)^2 \tag{14}$$

where $m_0$, $a$, and $n$ are the power-law constant, the temperature sensitivity, and the power-law index, respectively. $I_2$ is the secondary invariant of the rate of deformation tensor.

The energy equation:

$$k_m \frac{d^2T}{dy^2} + \tau_{xy} \frac{dv_x}{dy} + \tau_{yz} \frac{dv_z}{dy} = 0 \tag{15}$$

and with the boundary condition:

When

$$y = 0, \quad v_z = v_x = 0$$

When

$$y = \delta, \quad v_z = V_b \cos\theta + A\omega \cos \omega t \ \sin\theta,$$
$$v_x = V_b \ \sin\theta + A\omega \ \cos \ \omega t \ \cos\theta$$

where $k_m$ is the thermal conductivity coefficient and $\delta$ is the depth of polymer melt.

To simplify these equations stated above, we assume that the pressure grads along $x$ and $z$ directions in the melt can be neglected (and thus it is $\partial P/\partial x = \partial P/\partial z = 0$). Moreover, as mentioned above, because of the existence of the vibration force field, the inertia term in the momentum equation cannot

be ignored. This means viscous dissipation heat becomes very important, which leads to a uniform temperature distribution in polymer melt. Also, the depth of screw channel is relatively thin compared with the diameter of screw; so the average temperature and the nominal shear rate can be used in the current calculation. Then, combining eqs. (10)–(14) yield:

$$\rho_m \frac{\partial v_z}{\partial t} - k_1 \frac{\partial^2 v_z}{\partial y^2} = 0 \tag{16}$$

$$\rho_m \frac{\partial v_x}{\partial t} - k_1 \frac{\partial^2 v_x}{\partial y^2} = 0 \tag{17}$$

$$k_1 = m_0 \ \exp\left[a\left(\frac{T_b - T_m}{2}\right)\right] \mathrm{I}_2^{(n-1)/2} \tag{18}$$

$$I_2 = \frac{\bar{V}_x^2 + \bar{V}_z^2}{\bar{\delta}^2} \tag{19}$$

where $\bar{\delta}$ is the average depth of polymer melt, and $\bar{V}_x$ and $\bar{V}_z$ can be obtained from the following deduction.

We assume the melt is flowing along a certain direction in the double-plate model, which is similar to that shown in Figure 2, the apparent viscosity is $\eta$, the nominal shear rate is $V/\bar{\delta}$, and the viscosity dissipation heat per unit time is $dW = \eta\left(V/\bar{\delta}\right)^2 dt$, which is assumed to be equal to that generated by a Newton liquid flowing in the same model with shear rate $\bar{V}/\bar{\delta}$, that is:

$$W = \frac{1}{T}\int_0^T \eta\left(V/\bar{\delta}\right)^2 dt = \eta\left(\bar{V}/\bar{\delta}\right)^2 \tag{20}$$

So, we obtain:

$$\bar{V}_x = \left(V_b^2 \ \sin^2\theta + \frac{1}{2}A^2\omega^2 \ \cos^2\theta\right)^{1/2} \tag{21}$$

$$\bar{V}_z = \left(V_b^2 \ \cos^2\theta + \frac{1}{2}A^2\omega^2 \ \sin^2\theta\right)^{1/2} \tag{22}$$

Considering the initial conditions:

$$\begin{cases} t = 0, \quad v_x = \frac{\left[1-\exp\left(-a_1\frac{y}{\delta}\right)\right]V_{bx}}{1-\exp(-a_1)}, \quad v_z = \frac{\left[1-\exp\left(-a_1\frac{y}{\delta}\right)\right](V_{bz}-V_{sz})}{1-\exp(-a_1)} \\ t = 0, \quad \frac{dv_x}{dt} = 0, \quad \frac{dv_z}{dt} = 0 \end{cases} \tag{23}$$

where

$$a_1 = \frac{a(T_b - T_m)}{n} \tag{24}$$

Using the Laplace-transform to solve the above equations, the velocity distribution in the polymer melt was obtained:

$$v_x = A\omega \ \cos\theta_b\left[6y \ \cos(\omega t) - \rho_m y^3\omega \ \sin(\omega t)/k_1\right]/(6\delta) + V_{bx}\, y/\delta \tag{25}$$

$$v_z = A\omega \ \sin\theta_b\left[6y \ \cos(\omega t) - \rho_m y^3\omega \ \sin(\omega t)/k_1\right]/(6\delta) + (V_{bz} - V_{sz})y/\delta \tag{26}$$

Substituting eqs. (12), (13), (25) and (26) into eq. (15) and considering the boundary conditions $T(0) = T_m, \ T(\delta) = T_b$, which lead to:

$$\left(\frac{dT}{dy}\right)_{y=0} = \frac{T_b - T_m}{\delta} + \frac{U_1}{k_m\delta} \tag{27}$$

where

$$\begin{aligned} U_1 = k_1\Big\{ & A^2\omega^2[\cos^2\omega t + (\rho_m\omega \ \sin\omega t/2k_1)^2\,\bar{\delta}^4/30 \\ & - \rho_m\omega\bar{\delta}^2\sin(2\omega t)/(24k_1)] + V_{bx}^2/2 + (V_{bz} - V_{sz})^2/2 \\ & + 2A\omega[V_{bx} \ \cos\theta_b + (V_{bz} - V_{sz}) \ \sin\theta_b]\ [\cos(\omega t)/2 \\ & - \rho_m\omega\bar{\delta}^2 \ \sin \ \omega t/(24k_1)]\Big\} \end{aligned} \tag{28}$$

Thereby, the heat flow $Q_1$ conducted out of the polymer melt into the interface between melt and solid-bed is:

$$Q_1 = k_m\frac{T_b - T_m}{\delta} + \frac{k_1 U_1}{\delta} \tag{29}$$

As shown in eq. (29), the heat flow $Q_1$ is fluctuating with time, therefore, an average value is necessary for calculating the length of the melting section and the solid bed distribution, which is:

$$\overline{Q}_1 = \int_0^{2\pi/\omega} Q_1 dt = k_m\frac{T_b - T_m}{\delta} + \frac{k_1\overline{U}_1}{\delta} \tag{30}$$

where

$$\begin{aligned} \overline{U}_1 = k_1\big\{ & A^2\omega^2[1/2 + \rho_m^2\omega^2\,\bar{\delta}^4/(240k_1^2)] \\ & + V_{bx}^2/2 + (V_{bx} - V_{sz})^2/2\big\} \end{aligned} \tag{31}$$

As mentioned above, as the thermal conductive coefficient of polymer material and the difference of temperature in the solid-bed (due to viscous dissipation heat) are comparatively small, hence, we assume that the heat flow $\overline{Q}_1$ is absolutely contributing to the melting of solid-bed, we have:

$$\overline{Q}_1 = 2\rho_s\lambda(W + H - 4\delta)\frac{d\delta}{dt} \tag{32}$$

where $\lambda$ is the latent heat of the polymer material, and $\rho_s$ is the density of polymer solid.

From the melting mechanism stated previously, the length of melting section is constant, and the average thickness of the polymer melts at one position along $z$ direction is unvaried. So, the time parameter $t$ can be expressed by $z$ and $V_{sz}(t = z/V_{sz})$, therefore, eq. (32) can be changed to:

$$\overline{Q}_1 = 2\rho_s\lambda(W + H - 4\delta)V_{sz}\frac{d\delta}{dz} \tag{33}$$

with the boundary conditions

$$z = 0 \qquad \delta = 0 \tag{34}$$

To simplify the calculation, substituting $\overline{\delta} = H/4$ into eq. (31), while considering the boundary conditions and solving eq. (33) yields:

$$z = \frac{2\rho_s\lambda V_{sz}}{k_m(T_b - T_m) + k_1^{'}U_1^{'}}\left[(W + H)\frac{\delta^2}{2} - \frac{4\delta^3}{3}\right] \tag{35}$$

where

$$U_1^{'} = k_1^{'}\Big\{A^2\omega^2[1/2 + \rho_m^2\omega^2H^4/(61440k_1^{'2})] + V_{bx}^2/2 + (V_{bx} - V_{sz})^2/2\Big\} \tag{36}$$

$$k_1^{'} = m_0\exp\left[a\left(\frac{T_b - T_m}{2}\right)\right]\left[16\frac{\bar{V}_x^2 + \bar{V}_x^2}{H^2}\right]^{(n-1)/2} \tag{37}$$

when $\delta = H/2$, the solid-bed disappears and the polymer melt fills the entire cross section of the screw channel. Hence, the length of melting section $z_T$ can be expressed by the following equation:

$$z_T = \frac{2\rho_s\lambda V_{sz}}{k_m(T_b - T_m) + k_1^{'}U_1^{'}}\left[(W + H)\frac{H^2}{8} - \frac{H^3}{6}\right] \tag{38}$$

substituting $\delta = W - X$ into eq. (35) leads to:

$$z = \frac{2\rho_s\lambda V_{sz}}{k_m(T_b - T_m) + k_1^{'}U_1^{'}}\left[(W + H)\frac{(W - X)^2}{2} - \frac{4(W - X)^3}{3}\right] \tag{39}$$

where $X$ is the distribution of the polymer solid-bed. Equation (39) is the analytical expression of the distribution of polymer solid-bed along the $z$ direction.

## EXPERIMENT

### Apparatus for experiment

The detail work principium of VISS extruder can be found in ref. 16 (U.S. Patent).

In the T-VISS extruder (Fig. 3), the barrel is made of a special material, which is transparent and can endure high (about 700°C) and low (about −10°C) temperatures. This allows the whole screw of the T-VISS extruder to be visible while operating so the melting process can be observed. Also, this equipment allows accurate recording of the length of the melting section at various operating conditions. The barrel of half-open barrel VISS extruder (H-VISS) can be opened easily (Fig. 4), and after using a forced convection cooling, the barrel is cooled and the polymer melt is frozen soon after the screw's rotation and vibration stops. Then, the material ribbon (Fig. 5) of the melting section is obtained. From the polymer ribbon, the basic flow pattern is traced back and the solid-bed distribution is obtained from the various cross sections by locating the boundaries between the molten and nonmolten areas; to avoid any ambiguities, small amounts of the solid feedstock is colored. Here carbon powder was used. A typical result of this procedure is obtained from our 20-mm H-VISS extruder with LDPE shown in Figure 6, where the vibration amplitude and frequency are 0.15 mm and 20 Hz, respectively. In Figure 6, the

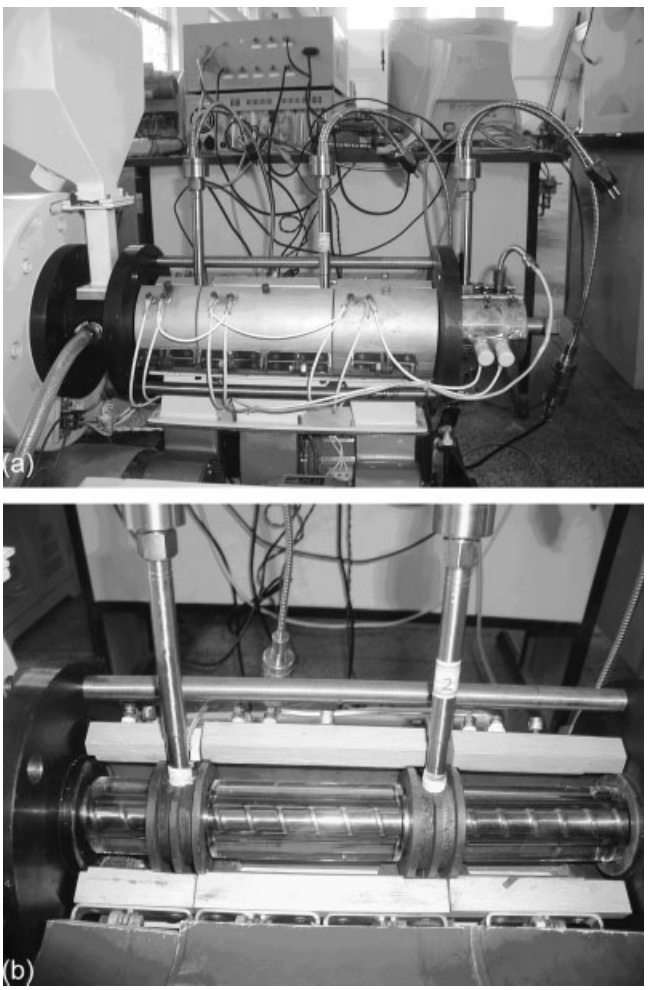


**Figure 3** Photo of the T-VISS extruder: (a) Side elevation; (b) Planform.

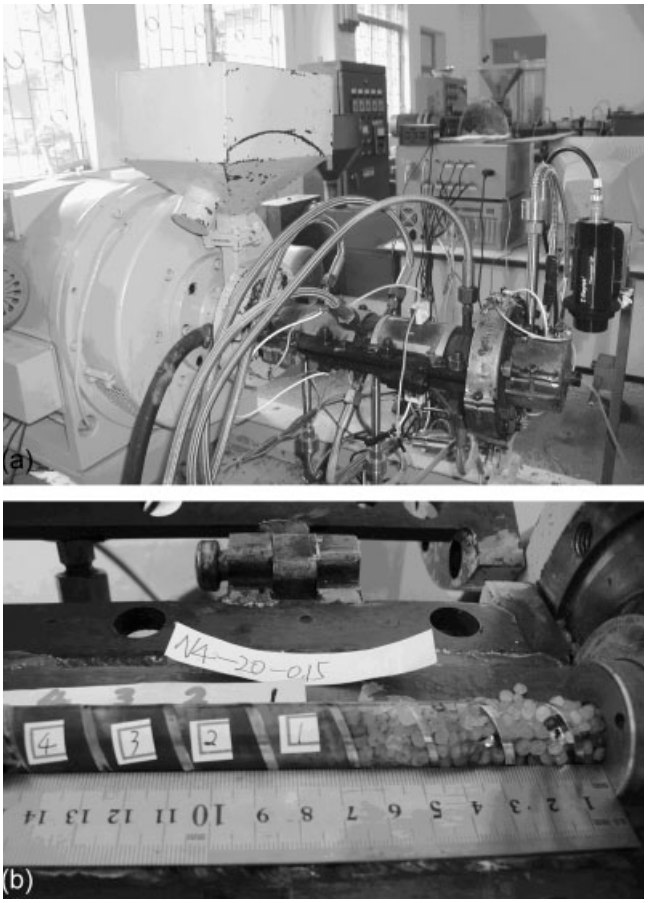


**Figure 4** Photo of the H-VISS extruder: (a) Photo of the entire extruder; (b) Photo of the screw and the opened barrel.

white part (a) of the material slice is the solid polymer, and the black part (b) is the polymer melt.

The screw of the T-VISS extruder and the H-VISS extruder have the same parameters given in Table I (where $D$ is the diameter of screw, θ is the helix

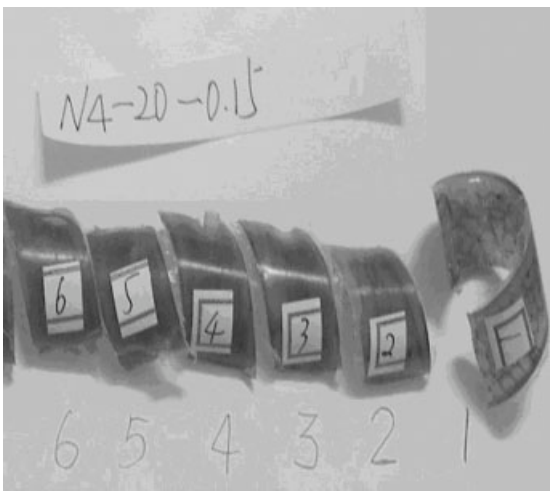


**Figure 5** LDPE material ribbon come from H-VISS extruder.

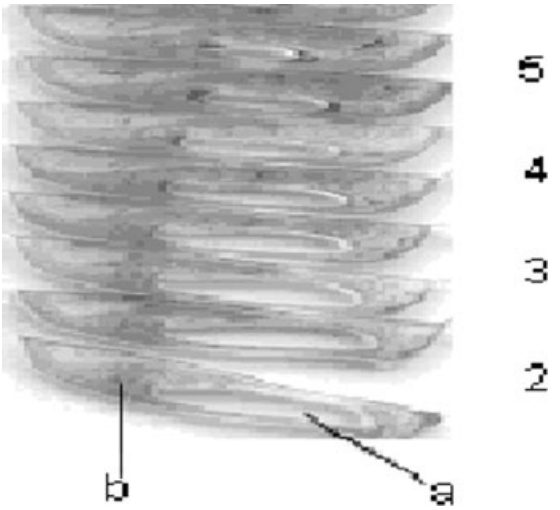


**Figure 6** Photo of the material slices (LDPE): $A = 0.15$ mm, $f = 20$ Hz; (a) Polymer solid-bed, (b) Polymer melt.

angle, $H$ is the depth of screw channel, $L$ is the length of screw, $W$ is the width of screw channel, and $e$ is the width of screw flight), and it can vibrate along axial direction as it is rotating as mentioned previously. The maximum values for frequency and amplitude of vibration can be up to 40 Hz and 2 mm, respectively.

### Material for experiment

The LDPE used for the experiment is 951-050, which was made in Petrochemicals, Maoming of China, and the physical properties are given in Tables II and III (the data for the physical properties is supplied by Petrochemicals, Maoming of China), where $\rho_s$ is the solid density, $T_g$ is the glass transition temperature, $k_s$ is the solid thermal conduction coefficient, $C_{ps}$ is the solid specific heat volume at constant pressure, λ is the latent heat, $\rho_m$ is the melt density, $T_m$ is the melting point, $k_m$ is the melt thermal conduction coefficient, and $C_m$ is the melt specific heat volume at constant pressure. The LDPE is in the form of flat ball with a diameter of about 3 mm. The parameters of power-law constitutive equation are: $m_0 = 5.6 \times 10^4$, $a = -0.01$, $n = 0.335$.

### Procedure for experiment

During the T-VISS extruder experiment, the temperature of the melting section, the melt conveying section, and the die are set at 140, 180, and 170°C,

**TABLE I**
**Parameter of Screw**

| $D$ (mm) | θ | $H$ (mm) | $L$ (mm) | $W$ (mm) | $e$ (mm) |
|---|---|---|---|---|---|
| 20 | 17.65° | 3.2 | 400 | 17 | 2 |

**TABLE II**
**Physical Properties of Solid LDPE (951-050)**

| $\rho_s$ (kg/m$^3$) | $T_g$ (°C) | $k_s$ (W/m °C) | $C_{ps}$ (kJ/kg °C) | λ (kJ/kg) |
|---|---|---|---|---|
| 915 | −68 | 0.335 | 2.76 | 129.8 |

respectively. When the temperature reaches the set value, the electromotor (supply screw rotation) and the oscillator (supply screw vibration) turn on, with the rotation speed controlled at 60 rpm. The frequency of the vibration is adjusted from 0 to 25 Hz (adjusted in 5-Hz intervals), and the amplitude from 0 to 0.8 mm (adjusted in 0.2-mm intervals). During each step, the length of the melting section and vibration parameters (frequency and amplitude) are recorded.

The temperature, the vibration parameters, and the rotation speed in the H-VISS extruder experiment are the same as that in T-VISS extruder experiment. During each step, the H-VISS extruder is running under steady conditions at a certain combination of vibration parameters for about 3 min, after which the electromotor and oscillator are then quickly stopped followed by rapid cooling of the barrel. When it is sufficiently cooled, the material ribbon (labeled with numbers in Fig. 5) is removed. Subsequently, the barrel is closed and the next experiment at different vibration parameters is performed. Finally, the material ribbons are cross-sectioned at various places and the material slices are derived. By measuring the geometric size of these slices, the polymer solid-bed distribution is obtained.

## RESULTS AND DISCUSSIONS

Figure 7 displays the melting process of T-VISS extruder. In Figure 7(a), the vibration frequency or amplitude is equal to zero (that is no introduction of vibration force field), contrast to Figure 7(b), where the frequency is 5 Hz and the amplitude is 0.15 mm. It is clear that, in Figure 7(a), the polymer solid is incompact and not uniform, and the melting section continues to about the 11 cm mark. However, in Figure 7(b), under the impact of vibration force field, the polymer solid-bed becomes more compact and uniform than in Figure 7(a) at the same position along the screw axis direction. Also, the melting section ends at about the 8 cm mark, a 27.28% decrease relative to Figure 7(a). From the comparison between

**TABLE III**
**Physical Properties of LDPE (951-050) Melt**

| $T_m$ (°C) | $k_m$ (W/m °C) | $C_m$ (kJ/kg °C) |
|---|---|---|
| 110 | 0.24 | 2.43 |

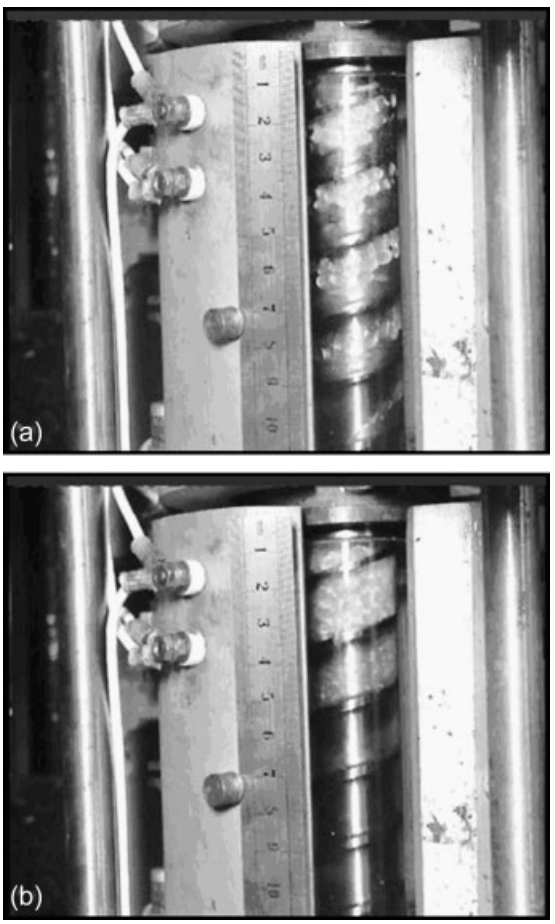


**Figure 7** Photo of the melting process of T-VISS extruder: (a) Without vibration-induced; (b) With vibration-induced (Frequency, 5 Hz; Amplitude, 0.15 mm).

the Figure 7(a,b), we can come to a conclusion that the introduction of vibration force field improves the melting process of an extruder.

The melting section lengths $z_T$ are plotted in Figure 8 as functions of vibration parameters. To

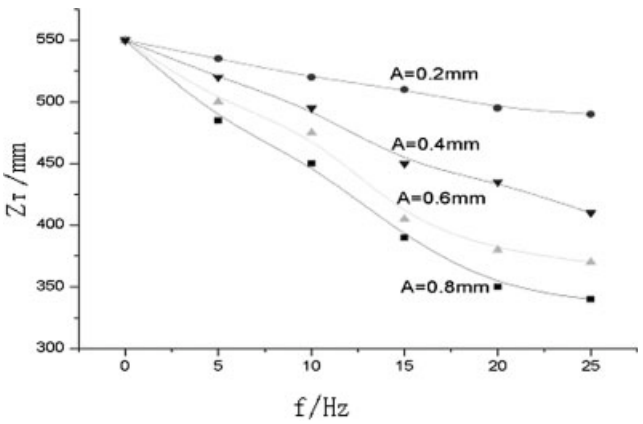


**Figure 8** Relationship between the length of melting section ($Z_T$) and the vibration parameters coming from experiment.

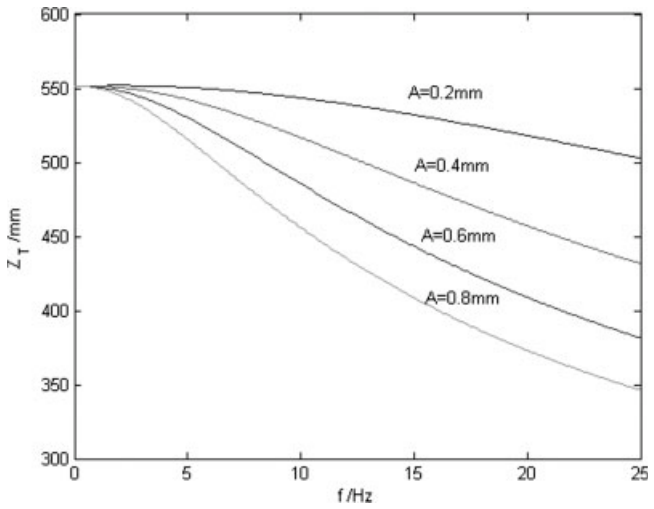


**Figure 9** Relationship between the length of melting section ($Z_T$) and the vibration parameters coming from theoretical calculation.

compare the theoretical calculation results, the melting section length $z_T$ is in the down screw channel direction. As shown in Figure 8, there are four curves representing the relationship between $z_T$ and $f$ ($f$ is the vibration frequency) for each amplitude ($A$ = 0.2, 0.4, 0.6, and 0.8 mm respectively, $A$ denotes the vibration amplitude). When $A$ = 0.8 mm and $f$ = 25 Hz, $z_T$ decreases to about 340 mm, which is a 38.2% decrease when compared to no vibration settings. Similarly, the $z_T$ decreases from about 550 mm to about 360, 420, and 500 mm under the condition that $A$ = 0.6, 0.4, 0.2 mm respectively. Further analysis shown in Figure 8 also reveals that, when $f$ = 20 Hz, the melting section length will decrease from about 510 mm to about 340 mm in traversing from $A$ = 0.2 to $A$ = 0.8 mm (a 33.3% decrease). When $f$ = 0, the value of $z_T$ shown in Figure 8 is the melting section length of conventional extruder

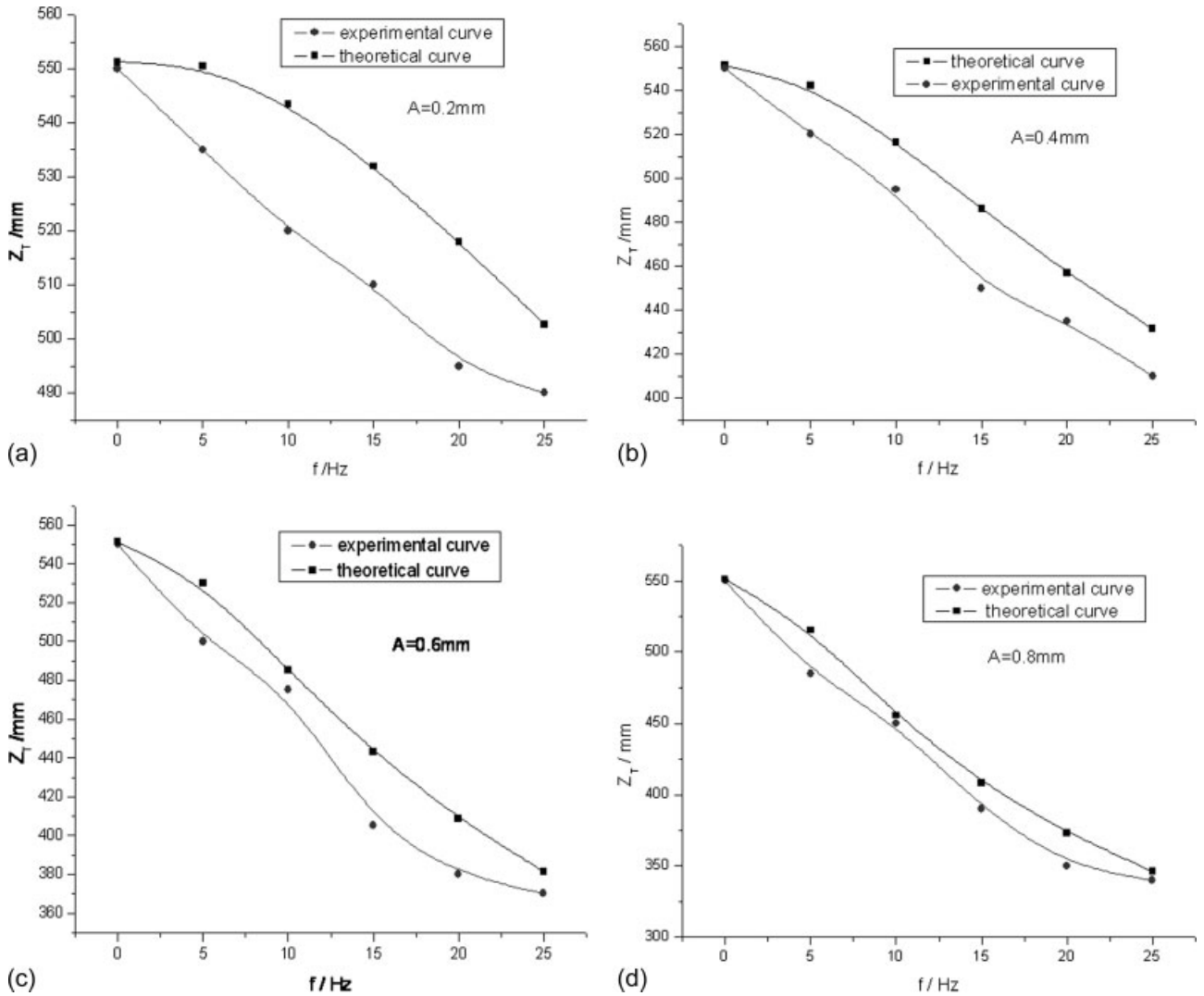


**Figure 10** Comparison illustrations of the melting section length coming from experiment and theoretical calculation: (a) $A$ = 0.2 mm, (b) $A$ = 0.4 mm, (c) $A$ = 0.6 mm, (d) $A$ = 0.8 mm.

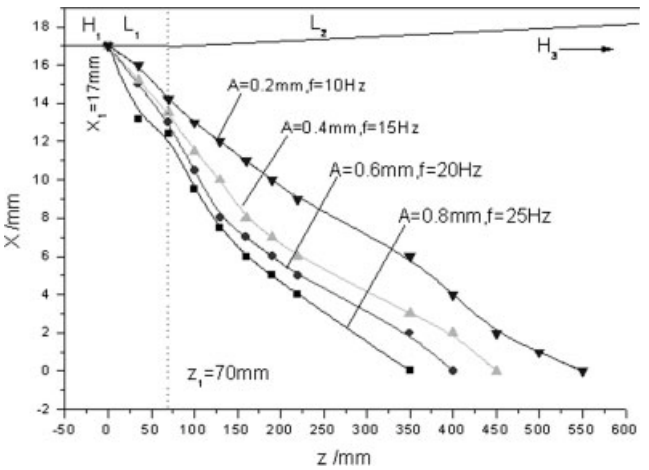


**Figure 11** Relationship between the solid-bed distribution and the vibration parameters coming from experiment.

(without vibration force field). The experimental results indicate that the melting section length of VISS extruder will decrease as the vibration parameters increases.

Figure 9 illustrates the relationship between the melting section length and the vibration parameters coming from the calculated theory [eq. (38)]. It can be clearly seen in Figure 9 that the increase of vibration amplitude and frequency can shorten the length of the melting section, which is in good agreement with the visual experimental results shown in Figure 8. As mentioned above, the intersection (about 555 mm) between the curve and the ordinate is the melting section length without vibration. As seen in Figure 9, when $f = 25$ Hz and $A = 0.8$ mm, the length is about 350 mm, which is decreased by 36.9%, and it is only a little less than the experimental value (38.2%). Figure 10 compares the melting section lengths from the actual experiment and theoretical calculation. It also shows that, the experimental results are very consistent with the theoretical calculation. However, there are some minor deviations seen in Figure 10(a). The reason is: To obtain the analytical expressions of the melting model during the theoretical deduction, many assumptions were made, which in reality are not totally neglected in the actual course of extrusion. On the other hand, test error is another reason for the deviation. Nevertheless, Figure 10(a–d) reveal that the theory is consistent with the experiment on the whole.

As mentioned above, the solid-bed distribution can be determined from the measuring of the geometric proportion between the solid and melt in the material slice as shown in Figure 6. The widths of the polymer solid-bed at various combinations of vibration parameters are shown as a function of $z$ ($z$ is in the down screw channel direction, and the starting point of the melting section is assumed at $z = 0$) in Figure 11. These four curves are the distribution of polymer solid-bed, and the starting point is the width of screw channel, where $z = 0$ (and thus it is the starting point of the melting section). In Figure 11, the declining rate of these curves increase as the vibration parameters increase, the intersections between these curves and the abscissa are the melting section length, which is consistent with Figure 8. As shown in Figure 11, it clearly explains that, the higher the vibration intensity, the faster the decreasing speed of the solid bed width ($X$) (and thus the increasing speed of the declining rate of the curves), when $X = 0$, the solid bed disappears and the screw channel is filled by polymer melt completely.

Figure 12 shows the course of melting along the screw channel direction in terms of the distribution of the solid bed. It is the same as what is shown in Figure 11, the abscissa $z$ is along the down channel direction, the $X$ ordinate represents the width of the solid bed. In agreement with our visual experiment, the declining rate of these curves (distribution of the solid bed) decreases as the vibration amplitude and frequency increase. Figure 13 is a comparison of the solid-bed distribution of the experiment and theoretical calculation (under various combinations of vibration parameters). As shown in Figure 13, when $A = 0.2$ mm, $f = 10$ Hz, and $z = 70$ mm, the solid bed width $X$ that comes from experiment is equal to 14 mm, and the $X$ that comes from theoretical calculation is equal to 14.4028 mm, the deviation between the two data is only 0.4028 mm (less than 3% error relative to experimental value).

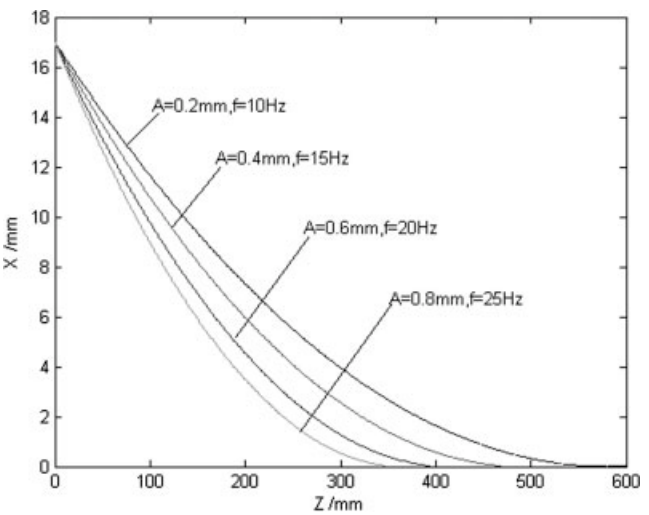


**Figure 12** Relationship between the solid-bed distribution and the vibration parameters coming from theoretical calculation.

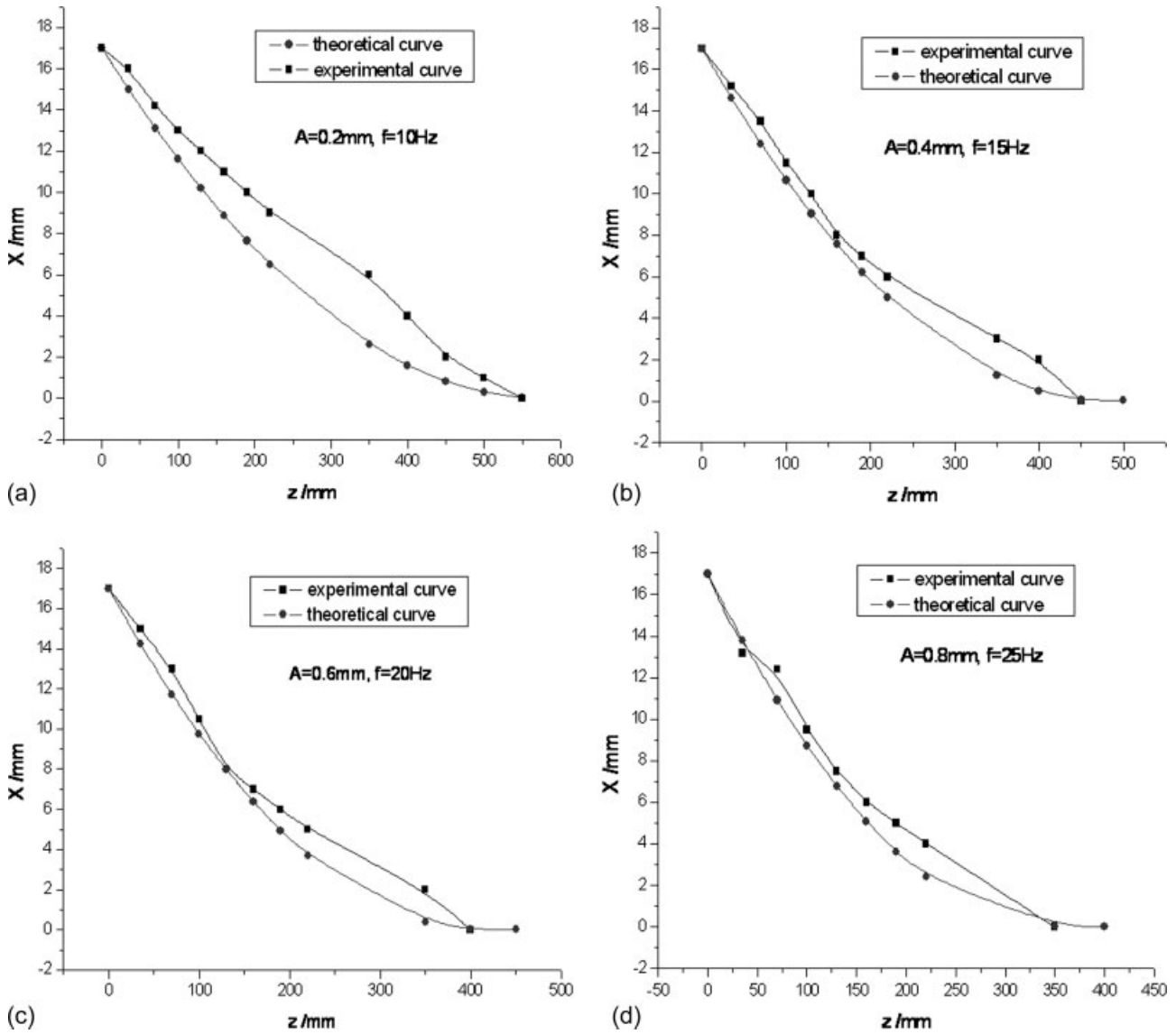


**Figure 13** Comparison illustration of the solid-bed distribution coming from experiment and theoretical calculation: (a) $A = 0.2$ mm, $f = 10$ Hz; (b) $A = 0.4$ mm, $f = 15$ Hz; (c) $A = 0.6$ mm, $f = 20$ Hz; (d) $A = 0.8$ mm, $f = 25$ Hz.

Figure 13(a–d) have proved that the theoretical model presented here is accurate, efficient, and applicable.

## CONCLUSIONS

The present mathematical model simulates the transport and melting phenomena in the melting zone of a VISS extruder where, in contrast to previous theories, a vibration force field is introduced during the whole course of the extrusion, the viscous dissipation has an important role in the melting process, the melt is considered to accumulate mainly in a film surrounding the solid bed rather than forming a significant pool at the flight wall. Also, the melt is flowing around the outside of the solid-bed as the melting proceeds. The comparison between the results of the experiment and the calculation sample indicates that the present model is accurate, efficient, and applicable. Also, it verifies that the introduction of vibration-induced field can improve the melting capacity of an extruder.

## References

1. Tadmor, Z. Polym Eng Sci 1966, 6, 185.
2. Tadmor, Z.; Klein, I. Engineering Principles of Plasticating Extrusion; Malbar, FL: Krieger, 1970.
3. Maddock, B. H. SPE J 1959, 15, 383.
4. Pearson, J. R. A.; Halmos, A. L.; Shapiro, J. Polymer 1976, 17, 905.
5. Shapiro, J.; Pearson, J. R. A.; Trottmow, R. Polymer 1978, 19, 1199.
6. Azhari, C. H.; Sahari, J.; Ing, L. Polymer 1998, 89, 4915.
7. Yung, K. L.; Xu, Y. Mater Process Technol 2001, 117, 21.

8. Yung, K. L.; Xu, Y.; Lau, K. H. Polymer 2002, 43, 983.
9. Menges, G.; Klenk, P. Kunststoffe 1967, 57, 677.
10. Dekker, J. Kunststoffe 1976, 66, 130.
11. Lindt, J. T. Polym Eng Sci 1976, 16, 284.
12. Lindt, J. T. Polym Eng Sci 1985, 25, 585.
13. Lee, K. Y.; Han, C. D. Polym Eng Sci 1990, 30, 665.
14. Wilczynski, K.; White, J. L. Polym Eng Sci 2003, 43, 1715.
15. Yichong, G.; Fuhua, Z. Polym Eng Sci 2003, 43, 306.
16. Qu, J. P. U.S. Pat. 5,217,302 (1993).
17. Wu, H. W.; Zhou, N. Q.; He, H. Z.; Qu, J. P. China Plastics 1996, 10, 53.
18. Peng, X. F.; Qu, J. P.; Li, L. F. EngPlaAP 1999, 27, 38.
19. Qu, J. P.; Qing, Y. M.; Tian, Y. C.; Zhou, N. Q. China Plastics Industry 2000, 28, 23.
20. Qu, J. P.; Chen, X. F. Light Industry Machinery 2004, 1, 21.
21. Feng, Y. Numerical simulation and experimental study of melting process in single screw extruder with vibration force field, Ph.D. Thesis, South China University of Technology, 2003; pp 31–39.